

A gas-phase “top-down” chemical link between aldehydes and alcohols

Christopher N. Shingledecker ^{1,*}, German Molpeceres ², A. Mackenzie

Flowers ³, Deaton Warren ¹, Emma Stanley ¹, and Anthony Remijan ⁴

¹Department of Chemistry, Virginia Military Institute, 24450 Lexington, VA, USA

²Departamento de Astrofísica Molecular, Instituto de Física Fundamental CSIC, Madrid, Spain

³Department of Chemistry, University of Virginia, 22904 Charlottesville, VA, USA

⁴National Radio Astronomy Observatory, 22903 Charlottesville, VA, USA

Correspondence*:

Germán Molpeceres

german.molpeceres@iff.csic.es

ABSTRACT

Introduction

Alcohols and aldehydes represent two key classes of interstellar complex organic molecules (COMs). This work seeks to better understand their possible chemical connections, with a focus on such molecules in the sources of the star-forming region Sgr B2 (N).

Methods

The gas-phase reaction between ethanol ($\text{CH}_3\text{CH}_2\text{OH}$) and the halogens fluorine and chlorine was investigated via DFT calculations, with the goal of determining whether astrochemically viable chemical pathways leading to acetaldehyde (CH_3CHO) exist. The studied reactions were then included in an astrochemical model of Sgr B2 (N) to determine their significance under real interstellar conditions.

Results

Our DFT calculations revealed that both chlorine and fluorine can react barrierlessly with ethanol to abstract a hydrogen atom. We further found that, following this initial step, the resulting ethanol radicals can undergo further reactions with atomic hydrogen, with some routes leading to acetaldehyde. Incorporation of these novel reactions in astrochemical models of hot cores suggest that they are indeed efficient under those conditions, and can lead to modest increases in the abundance of CH_3CHO during model times where gas-phase ethanol is abundant. Of the ethanol radicals included in our chemical network, we found CH_3CHOH to have the highest abundances in our simulations comparable to that of ethanol at some model times.

Discussion

Overall, this work reveals a novel gas-phase ‘top-down’ link from alcohols to aldehydes that complements the better studied ‘bottom-up’ routes involving grain-surface H-addition reactions yielding alcohols from aldehydes. Moreover, results from our astrochemical models suggest that the ethanol radical CH_3CHOH may be detectable in the interstellar medium.

Keywords: astrochemistry, Sgr B2, DFT, astrochemical modeling, alcohols, aldehydes, halogens

1 INTRODUCTION

Hot cores, especially those found towards the Galactic Center in the Sagittarius (hereafter Sgr) B2 (N) complex, are known to be some of the most chemically rich interstellar sources (Belloche et al., 2013; Bonfand et al., 2019; Neill et al., 2014; Loomis et al., 2013; Zaleski et al., 2013). The reason for this complexity is manyfold, though significant factors include the fact that the higher temperatures obtained during core warmup liberate existing complex organic molecules (COMs) already present in dust-grain ice mantles out to the grain surfaces and into the gas-phase (Yang et al., 2022; McClure et al., 2023). This enables a comparatively brief but active period of surface chemistry due to the enhanced mobility of surface species heavier than hydrogen (Garrod et al., 2008; Ioppolo et al., 2020; Qasim et al., 2020).

Underscoring this chemical complexity is the fact that molecules bearing most of the functional groups in organic chemistry have now been detected (McGuire, 2018), with many more being detected annually. Of these, two of the most important and common are alcohols and aldehydes, having R-OH and R-CHO groups, respectively, where R could be any other part of the molecule. One of the essential tasks in astrochemistry is investigating possible chemical connections between detected molecules. Alcohols and aldehydes hold a crucial cornerstone in the evolution of chemical complexity in the ISM, bearing two of the most chemically ubiquitous functional groups. To this end, a number of studies have focused on the chemical connections between alcohols and aldehydes, for example, the theoretical studies of Woon (2002), Rimola et al. (2014), Das et al. (2008), Song and Kästner (2017) and Mondal et al. (2021), as well as the experimental work by Qasim et al. (2019) and Hiraoka et al. (1998). Most of these studies envisioned the formation of the alcohol from the aldehyde via successive reactions with atomic hydrogen on grain surfaces, which represents a “bottom-up” chemical link between the two. This hypothesis is supported by the easy hydrogenation of formaldehyde H_2CO to methanol CH_3OH (Watanabe and Kouchi, 2002).

While the “bottom-up” route is well supported for methanol and formaldehyde, the picture is more complicated for acetaldehyde and ethanol. Recent computational works suggest that grain-surface formation routes of acetaldehyde are likely to be unfavorable (Perrero et al., 2023). This, combined with the presence of acetaldehyde in cold prestellar cores (Scibelli and Shirley, 2020), points to the main mechanisms of acetaldehyde formation potentially being in the gas-phase (Vazart et al., 2020). Further complicating the bottom-up scenario, results from recent quantum chemical calculations by Molpeceres et al. (2025) suggest that acetaldehyde, at least, is resistant to further hydrogen addition, complicating the bottom-up scenario.

Another possible chemical link between alcohols and aldehydes is a “top-down” route where alcohols are converted to aldehydes through successive hydrogen abstractions. To further investigate the role of gas-phase formation, it is this chemical route that this work seeks to address through a combination of ab initio quantum chemical calculations and astrochemical modeling of Sgr B2(N). However, rather than assuming a series of reactions with, initially, the alcohol with H, we instead assume the initiating co-reactant are the halogen atoms Cl and F in the gas-phase. This choice was motivated in part by the observation by Balucani et al. (2015) of the increased reactivity of these species compared with H. Both HCl and HF have been detected towards Sgr B2 (Zmuidzinas et al., 1995; Neufeld et al., 1997), with observed fractional abundances that exist in the ranges of $\sim 10^{-10}$ – 10^{-9} relative to molecular hydrogen. The contributions of chlorine and fluorine chemistry in the context of astrochemical models have previously been studied in various interstellar environments in Acharyya and Herbst (2017), wherein they include reactions of methanol with atomic F and Cl, which can result in either the CH_3O or CH_2OH radical. In the case of

the latter, the CH_2OH can react further with a chlorine atom to produce formaldehyde in the “top-down” fashion, but reactions including ethanol were not investigated (Acharyya and Herbst, 2017).

The rest of this paper is structured as follows: in §Methods we describe our approaches for both the quantum calculations and the astrochemical modeling, in §Results & Discussion we present the results of this work, and finally, we summarize our findings in §Conclusions.

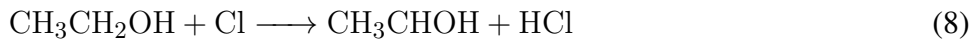
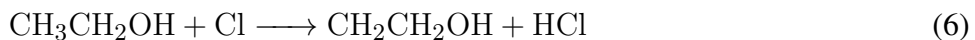
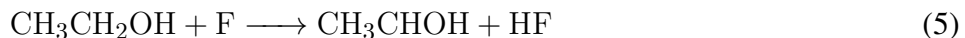
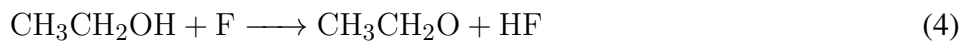
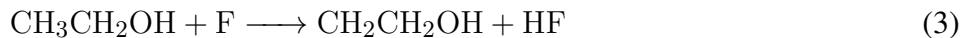
2 METHODS

2.1 Quantum Chemical Calculations

We determined the outcome of the H-abstraction reactions with fluorine, shown in Eq. (1), and chlorine, shown in Eq. (2):



using quantum chemical calculations. The first step is to determine the stationary points in each of the potential energy surface (PES) (Section 2.1.1) for the different reaction channels, namely:



Later, we derive the corresponding bimolecular rate constants of each of the reaction channels (Section 2.1.2), that we later introduce in the kinetic models of Sgr B2 (N).

2.1.1 Characterization of Stationary Points

All geometries were optimized using density functional theory (DFT) with the double-hybrid functional rev-DSD-PBEP86(D4) (Kozuch and Martin, 2011; Santra et al., 2019; Caldeweyher et al., 2019), in combination with the cc-pCVTZ basis set (Hill et al., 2010), which includes functions designed to account for core–valence correlation. Zero-point vibrational energy (ZPVE) corrections were computed within the harmonic approximation by numerical differentiation of the gradient. To obtain more accurate energetics, we refined the energy of each stationary point at the CCSD(T)/cc-pCVTZ level (Raghavachari et al., 1989; Bartlett et al., 1990; Hill et al., 2010) using an unrestricted Hartree-Fock (UHF) reference wavefunction (Neese, 2000). All calculations, including geometry optimizations, ZPVE corrections, and single-point energy refinements, were performed correlating all electrons, i.e., without applying the frozen-core approximation. All our electronic structure calculations employ the ORCA package (v.6.0.0) (Neese et al., 2020a,b; Neese, 2022).

To investigate the reactivity of each distinct hydrogen atom in ethanol, we performed exploratory PES scans along well-defined reaction coordinates, followed by full optimization of the resulting stationary points. All reactions were modeled (Section 2.1.2) within a general mechanistic framework involving two van der Waals complexes: one preceding the hydrogen abstraction (pre-reactive complex, PRC) and one following it (post-reactive complex). This scheme was applied to all possible hydrogen abstraction pathways, regardless of whether the corresponding transition states (TS) were submerged. The only exception was the set of reactions $\text{CH}_3\text{CH}_2\text{OH} + \text{F/Cl} \longrightarrow \text{CH}_3\text{CHOH} + \text{HF/HCl}$, where PES scans were inconclusive, suggesting a barrierless abstraction mechanism with no PRC on the electronic energy surface at the rev-DSD-PBEP86(D4)/cc-pCVTZ level. To assess whether these reactions truly proceed without an activation barrier, as proposed in previous studies (Taketani et al., 2005), we carried out nudged elastic band (NEB) calculations (Henkelman et al., 2000) to confirm a strictly downhill energy profile. The NEB paths were discretized into 24 images including endpoints and computed using the KNARR module of the ASH library (Asgeirsson et al., 2021; Bjornsson, 2022).

2.1.2 Kinetic Calculations

We compute phenomenological rate constants for all bimolecular channels considered in this study using an ab initio transition state theory master equation (AITSTME) framework. Barrierless processes, such as capture into a pre-reactive complex (PRC) or into a product-side van der Waals (vdW) complex, as discussed above, and the escape from product vdW complexes are modeled using phase space theory (Pechukas and Light, 1965; Chesnavich, 1986). The rigid scans for these barrierless association and dissociation channels are performed at the spin component scaled MP2 (SCS-MP2) level (Grimme et al., 2012) with the aug-cc-pVTZ basis set (Kendall et al., 1992), starting from the corresponding stationary point on the potential energy surface (on the pre-optimized geometries using the double hybrid functional). The scans extend from 4 Å to 15 Å to capture the long range asymptotic behavior of the interactions. This last set of calculations were carried out within the frozen core approximation. The resulting scan energies are fitted to a potential of the form $V(r) = -C/r^n$, with $n = 6$ for entrance channels and $n = 5$ for exit channels. The choice of using a fit with $n = 5$ stems from the change in the nature of the interaction once HF or HCl are formed. While the entrance channel corresponds to an atom–molecule interaction well described by an r^{-6} dependence, the exit channels are dominated by dipole–dipole interactions, better represented by an r^{-5} behavior. In fact, the large dipole moment of HF (or HCl) can make some exit channels even better reproduced by an $n = 4$ dependence. Nevertheless, we retain $n = 5$ for consistency, since the kinetics of the reaction of interest are mainly governed by the capture event, for which the r^{-6} fit provides a good description in all cases (Figure 1). In cases where a barrier exists between the PRC and the product vdW complex, the interwell transition is modeled using RRKM theory, including tunneling corrections based on asymmetric Eckart transmission coefficients. To avoid numerical instabilities arising from vibrational entropy contributions, all vibrational frequencies of weakly bound complexes below 100 cm⁻¹ are raised to that threshold. The elementary rate constants and the resulting phenomenological rate constants for the full process are calculated using the MESS code (Georgievskii et al., 2013), across a temperature range of 30 to 500 K and at a residual pressure of 1×10^{-7} atm, low enough to prevent collisional relaxation of the PRC and product vdW complexes. Finally, in a first approximation we consider that all reactions take place in the lowest conformer of ethanol, that is, we do not consider a multistate (or multiconformer) treatment of the reaction (Zheng and Truhlar, 2012).

The phenomenological rate constants are later fitted to a typical 3-parameter Arrhenius-Kooij formula of the type:

$$k = \alpha \left(\frac{T}{300\text{K}} \right)^\beta \exp \left(-\frac{\gamma}{T} \right) \quad (9)$$

where α is the pre-exponential factor for the rate coefficient, β gives the temperature dependence, and γ is the energy barrier. The resulting fits to this equation for reactions (3) - (8) are described below.

2.1.3 Avenues for the improvement of the quantum chemical calculations

The model chemistry employed in our electronic structure calculations is sufficiently accurate for the purposes of this study. Nevertheless, several refinements could be implemented to achieve a fully quantitative description of the reactions, particularly at higher temperatures where finite-temperature effects may influence the kinetics. Possible improvements include going beyond the harmonic approximation to account for anharmonic vibrational frequencies, explicitly considering ethanol conformational effects, or introducing methodological refinements to the model chemistry, such as enlarging the basis set. The kinetic treatment could also be improved by moving beyond a one-dimensional zero-curvature tunneling correction to more accurately capture corner-cutting effects (Nandi et al., 2022). Finally, the most immediate avenue for improvement would be a more accurate description of the capture event in the barrierless channels, since capture theory is known to overestimate the capture rate constant (Marchione et al., 2022; Tsikritea et al., 2022).

2.2 Astrochemical Modeling

In order to estimate the efficiency of the studied reactions under real astrophysical conditions, astrochemical models were run. For this, the *nautilus* v1.1 code was used (Riaud et al., 2016). The physical conditions used in the model, shown in Table 1, were chosen to replicate those of Sgr B2 (N). Briefly, a three-phase (gas, grain surface, and grain bulk) three stage (collapse, warm up, and constant physical conditions) model was employed to simulate the collapse of a prestellar cloud and the formation of a hot core (Garrod, 2013). The initial physical conditions at the beginning of collapse include an A_V of 0.3, density of 10^3 cm^{-3} . The collapse stage has a duration of $8 \times 10^5 \text{ yr}$, at the end of which the model reaches a density of 10^8 cm^{-1} , as shown in Fig. 3. During the collapse, the gas temperature was held at a constant value of 10 K and the grain temperature, which starts at 15 K, becomes coupled to the gas temperature of 10 K by the end of this first stage, which can be seen in Fig. 2. A cosmic ray ionization rate of $\zeta = 1.3 \times 10^{-16} \text{ s}^{-1}$ was used for all stages to account for the enhanced cosmic ray flux in the Galactic Center, which is likely at least one order of magnitude greater than the standard value of $\sim 10^{-17} \text{ s}^{-1}$ (Goto, 2013).

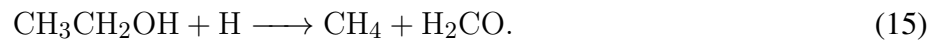
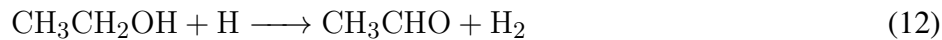
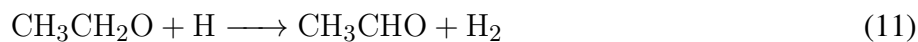
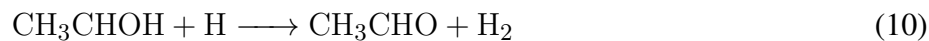
Table 1. Physical parameters used in all astrochemical models. Note: the parameter α is the chemical desorption efficiency (Garrod et al., 2007).

Parameter	Value
ζ	$1.3 \times 10^{-16} \text{ s}^{-1}$
UV Flux	1 Draine
α	1.0×10^{-2}
Grain Radius	$1.0 \times 10^{-5} \text{ cm}$
Diffusion barrier width	$1.0 \times 10^{-8} \text{ cm}$
Surface site density	$1.5 \times 10^{15} \text{ sites/cm}^2$
E_b^{surface}/E_D	0.4

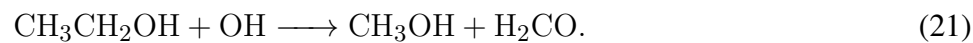
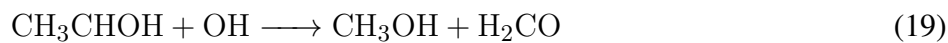
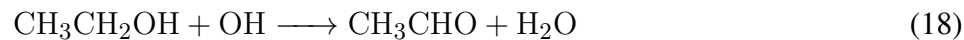
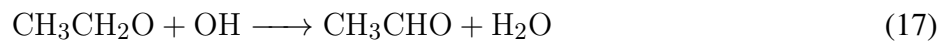
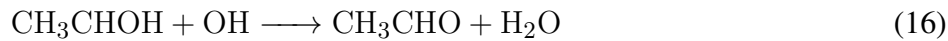
Following the collapse stage, a warm up occurs, during which the density and A_V remain constant while, as shown in Fig. 2, the gas and grain temperatures rise to ~ 400 K over a period of $\sim 10^6$ yr. Finally, after the warm up stage, the model continues with static physical conditions until a total model time of 10^7 yr is obtained.

Initial elemental abundances were taken from Laas and Caselli (2019), and correspond to known cosmic standard elemental abundances. The full table of values is given in Laas and Caselli (2019), but we note in particular an initial chlorine abundance of 2.88×10^{-7} relative to hydrogen (Esteban et al., 2004) and fluorine abundance of 3.63×10^{-8} relative to hydrogen (Asplund et al., 2009). These values differ slightly from those used in Acharyya and Herbst (2017), which used initial abundances relative to hydrogen of 1×10^{-7} and 1.8×10^{-8} of chlorine and fluorine, respectively. To determine if the differences in initial abundances will affect the overall chemistry, additional models were run with starting with initial abundances of 10^{-7} and 1.8×10^{-8} for chlorine and fluorine, respectively.

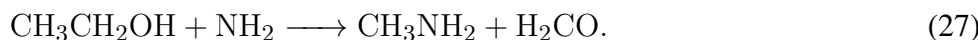
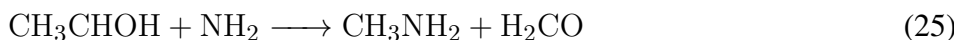
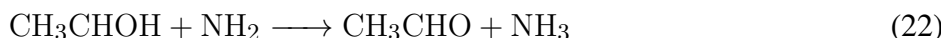
The base chemical network used here is that of Byrne et al. (2024), developed for work by the GOTHAM (GBT Observations of TMC-1 Hunting Aromatic Molecules) project. To this was added reactions (3) - (8), in addition to a number of destruction paths for the ethanol radicals with H, OH, and NH₂. The destruction reactions with H added to our network are given in Equations (10) - (15), namely,



Equations (16) - (21) show those with OH,



Finally, Equations (22) - (27) give the destruction reactions with NH₂, which are as follows:



All of the above destruction reactions were assumed to occur barrierlessly at the collisional rate of $10^{-10} \text{ cm}^3 \text{ s}^{-1}$, split between the two product channels, corresponding to H abstraction (in the case of reactions leading to acetaldehyde) vs attack of the alpha carbon. Our choice of rate coefficient is a typical approximate value for barrierless bimolecular gas-phase reactions without significant long-range forces, though follow up studies of these reactions are needed to confirm this choice, a task beyond the scope of this work. If these destruction reactions prove to be less efficient, the abundance of the intermediate radicals would be higher, which would have implications related to their detectability as described below. If the reverse is true, then the chemical connections between alcohols and aldehydes is further strengthened. Either outcome would be of astrochemical interest.

3 RESULTS & DISCUSSION

3.1 Quantum Chemical Results

3.1.1 $\text{CH}_3\text{CH}_2\text{OH} + \text{F}$

The PES profiles for H abstraction by fluorine at the three inequivalent positions are shown in Figure 4. A quick inspection of the graph reveals that all hydrogen abstraction reactions with fluorine (Reactions 3, 4, and 5) are barrierless with respect to the reaction asymptote $\text{CH}_3\text{CH}_2\text{OH} + \text{F}$. It is important to note, however, that each reaction is barrierless for a different reason. In the case of Reaction 3, we located a TS on the electronic energy surface (that is, without ZPVE correction) at less than $1.0 \text{ kcal mol}^{-1}$. This shallow barrier disappears upon application of ZPVE. We therefore consider this reaction to be effectively barrierless, proceeding directly toward the van der Waals product complex (VDW1 in Figure 4). Nevertheless, a small barrier might still be present if more accurate electronic structure methods were used to determine the stationary point energies. For Reaction 4, the barrierless character originates from the submersion of the TS below the reactant asymptote. This is due to the stabilization of the PRC, located at approximately $-3.6 \text{ kcal mol}^{-1}$, which consequently lowers the energy of the TS as well. Finally, Reaction 5 is the only case that is entirely barrierless, displaying a strictly downhill energy profile on the electronic PES. This behavior is confirmed by the NEB calculations described in Section 2.1.1.

The PES profiles shown in Figure 4 provide a useful framework to interpret the kinetics of these reactions. The corresponding rate constants are presented in Figure 5 (top panel). Both Reactions 3 and 5 exhibit clearly barrierless behavior, with only a minor dependence on temperature. We attribute this slight temperature dependence to the small enhancement of the final step, VDW \rightarrow Product, at higher temperatures. In contrast, Reaction 4 shows anti-Arrhenius behavior, which is typically observed

in barrierless reactions where the redissociation from the PRC back to reactants becomes increasingly significant at higher temperatures.

3.1.2 $\text{CH}_3\text{CH}_2\text{OH} + \text{Cl}$

The $\text{CH}_3\text{CH}_2\text{OH} + \text{Cl}$ reaction is slower than its fluorine analogue. This fact follows directly from the PES cuts in Figure 6. Among the three abstraction pathways, only Reaction 8 is truly barrierless, as confirmed by an NEB calculation, exactly as for the corresponding F reaction. The remaining pathways, Reactions 6 and 7, display well defined TSs above the reactant asymptote, which strongly diminish their rates. The absolute PES profile agrees closely with earlier work on this system (Taketani et al., 2005). It reproduces both the small exothermicity of Reaction 6 and the endothermicity of Reaction 7, the latter making that channel relevant only at high temperature. PRC1 (Reaction 6) and PRC2 (Reaction 7) show inverted stability with respect to their products $\text{CH}_2\text{CH}_2\text{OH}$ and $\text{CH}_3\text{CH}_2\text{O}$. PRC2 is stabilised by H bonding between the hydroxyl group of $\text{CH}_3\text{CH}_2\text{OH}$ and the Cl atom, making it the most stable PRC in this study and even more stable than PRC2 of Reaction 4. Such deep stabilisation raises the overall barrier for Reaction 7, leading to very slow kinetics. By contrast, Reaction 6 has a much lower barrier; although slower than the barrierless channel (Reaction 8), its rate constants exceed those of Reaction 7 by several orders of magnitude at low temperature. The stabilization of PRC2, in principle, leads to competition between back-dissociation to the reactants and evolution through a roaming mechanism toward VDW3, ultimately forming $\text{CH}_3\text{CHOH} + \text{HCl}$. Our simplified kinetic scheme does not take roaming into account, which may result in an underestimation of the overall rate constant. However, this approximation partially compensates for the possible presence of sub-kcal mol⁻¹ activation barriers for reaction 8, which would otherwise artificially enhance the calculated rate at low temperatures.

Looking at the rate constants for the $\text{CH}_3\text{CH}_2\text{OH} + \text{Cl}$ reaction, shown in Figure 5 (bottom panel), we observe that, in contrast to the case with fluorine, the reactivity is entirely dominated by the channel corresponding to Reaction 8. This is unsurprising given its barrierless nature. However, although irrelevant for the overall kinetics, we also find that the gap in rate constants between Reactions 6 and 7 decreases with increasing temperature, and the two channels converge at high temperature. This unexpected trend can be rationalised by a combination of two effects. First, the greater thermal energy at high temperature makes the endothermic $\text{CH}_3\text{CH}_2\text{O} + \text{HCl}$ channel (Reaction 7) accessible, while it is effectively closed at low temperature. Second, the higher imaginary frequency of the TS in Reaction 7 (2013*i*) compared to that of Reaction 6 (1042*i*) enhances the tunneling efficiency, as this frequency can be taken as an estimate of the crossover temperature for tunneling (Gillan, 1987), which is significantly higher for Reaction 7. Nonetheless, as noted above, this behaviour does not affect the global kinetics, since both Reactions 6 and 7 remain minor channels compared to the dominant Reaction 8.

3.1.3 Comparison between reactions with fluorine and chlorine

The comparison between the two reactions studied in this work reveals fundamental differences between H abstraction by fluorine and by chlorine, which are worth highlighting to guide further chemical interpretation. As expected from basic principles of inorganic chemistry, fluorine is overall more reactive than chlorine. However, in this case we can quantify the effect. Considering the sum of all reaction channels at low temperatures $8.85 \times 10^{-10} \text{ cm}^{-3} \text{ s}^{-1}$, we find that the total rate constant for the fluorine system is approximately a factor 2–3 (2.8) larger than that for chlorine. The anti-Arrhenius behavior of Reaction 4, together with a slightly faster capture efficiency in Reaction 8 compared to Reaction 5 prevent the system from reaching the theoretical factor of three that would be expected based solely on the number of barrierless channels. It is also worth noting that while all reactions involving H abstraction by fluorine

are strongly exothermic, this is not the case for chlorine, which shows much lower exothermicities and even endothermic channels at low temperatures, as in the case of Reaction 7. This difference suggests caution when extrapolating the behavior of chlorine to other systems or when proposing new H-abstraction reactions involving chlorine.

3.2 Astrochemical Modeling

Table 2. Fitted parameters of equation 9 for the reactions considered in our quantum chemical calculations. The fit is performed for the rate constants derived between 30-500 K.

Reaction	Label	α ($\text{cm}^{-3} \text{s}^{-1}$)	β	γ (K)
$\text{CH}_3\text{CH}_2\text{OH} + \text{F} \longrightarrow \text{CH}_2\text{CH}_2\text{OH} + \text{HF}$	3	4.0(-10)	1.7(-1)	9.8(-3)
$\text{CH}_3\text{CH}_2\text{OH} + \text{F} \longrightarrow \text{CH}_3\text{CH}_2\text{O} + \text{HF}$	4	6.1(-11)	-1.4(0)	4.5(1)
$\text{CH}_3\text{CH}_2\text{OH} + \text{F} \longrightarrow \text{CH}_3\text{CHOH} + \text{HF}$	5	4.1(-10)	1.7(-1)	1.3(-3)
$\text{CH}_3\text{CH}_2\text{OH} + \text{Cl} \longrightarrow \text{CH}_2\text{CH}_2\text{OH} + \text{HCl}$	6	4.6(-13)	2.6(0)	-1.9(2)
$\text{CH}_3\text{CH}_2\text{OH} + \text{Cl} \longrightarrow \text{CH}_3\text{CH}_2\text{O} + \text{HCl}$	7	7.4(-12)	-4.4(-1)	5.2(2)
$\text{CH}_3\text{CH}_2\text{OH} + \text{Cl} \longrightarrow \text{CH}_3\text{CHOH} + \text{HCl}$	8	4.6(-10)	1.7(-1)	5.3(-2)

In Table 2 we show the values of the Arrhenius-Kooij parameters used to introduce the halogen-mediated H-abstraction reactions considered in Section 3.1. Calculated abundances for acetaldehyde (CH_3CHO) for our three-stage model of Sgr B2(N) are shown in Fig. 7. Shown in yellow are results from our “control” model, which uses the unmodified network of Byrne et al. (2024) without any of the new reactions mentioned in this work¹. The blue curve in the figure gives the model results using our newly expanded chemical network. A comparison of the two shows that they are largely the same, save for a noticeable increase in acetaldehyde abundance around a model time of 10^6 yr.

To examine the effect of variations in initial Cl and F abundances, we ran a model using the lower initial abundances for chlorine and fluorine of, respectively, 10^{-7} and 1.8×10^{-8} relative to hydrogen. These values have been used in previous investigations of halogen astrochemistry by, e.g., Neufeld et al. (2005) and Acharyya and Herbst (2017). As can be seen in Fig. 7, the reduced halogen abundances have only a minor influence on the time-dependent abundances of CH_3CHO , with the peak abundance remaining unchanged.

The increase in acetaldehyde abundance provides a clue as to the underlying chemistry. The likely answer is implied in Fig. 8. Around 10^6 yr in the model, the gas (and dust) temperature is roughly 175 K, as shown in Fig. 2. It is at this point that ethanol, which has hitherto been trapped mostly on grains, is efficiently liberated into the gas. This occurrence becomes the occasion for our new reactions to show their utility, when the desorbed ethanol begins reacting with F and Cl to produce the three ethanol radicals. Of the three, CH_3CHOH is the most abundant, reaching approximately the abundance of its ethanol precursor from a few times 10^5 to 10^6 yr.

In previous work done investigating the role of fluorine and chlorine in the chemistry of various interstellar environments (including hot cores), Acharyya and Herbst (2017) included a system of F and Cl reactions in their chemical network, including those where atomic F and Cl react with methanol. From Table 2 and Fig. 5, we find that the temperature-dependent rate constants for reactions 3 – 8 reach into the range of $\sim 10^{-13}$ – $5 \times 10^{-10} \text{ cm}^3 \text{ s}^{-1}$. Comparing these to the chlorine and fluorine reactions with methanol, as summarized in Acharyya and Herbst (2017), the ethanol pathways show a slight increase in reactivity. The

¹ <https://zenodo.org/records/13257329>

most favourable pathway for the methanol-halogen reactions is found in the $\text{CH}_3\text{OH} + \text{F}$ channel resulting in CH_2OH , with a rate constant of $k = 1.66 \times 10^{-10} \text{ cm}^3 \text{ s}^{-1}$ (Jodkowsky et al., 1999).

Despite reactions 6 and 7 not having rate constants reaching as high of values and exhibiting clear barriers, the remaining four reactions all have peak values that are at least a factor of 2 larger than their methanol counterparts Acharyya and Herbst (2017). Furthermore, reactions 3 and 8 both share similar peak values, combined with their overall barrierless nature, this suggests that both chlorine and fluorine can efficiently contribute to the presence of the CH_3CHOH radical.

Our calculated abundance presents the interesting possibility for the detection of CH_3CHOH in interstellar environments, however, to the best of our knowledge, no laboratory spectrum for this species exists, though a recent study by Williams et al. (2021) did report calculations of relative energetics. Measured laboratory spectra generally provide a more reliable basis for astronomical searches than theoretically calculated spectra. We estimate that the strongest predicted transitions may appear in the radio to centimeter range (typical of cold dark clouds) or in the millimeter to submillimeter range (typical of hot molecular cores). Given its structural similarity to both $\text{CH}_3\text{CH}_2\text{OH}$ and CH_2CHOH - two well-characterized interstellar molecules — it is plausible that the CH_3CHOH radical is also present in astronomical environments. Completing the connection, the ethanol radicals, once formed, react with predominantly H to yield the spike in acetaldehyde abundance observed in Fig. 7. Thus, our model results show that, in times and places where gas-phase ethanol is present, our new destruction reactions with halogens represent efficient pathways linking alcohols and aldehydes.

4 CONCLUSIONS

In this work, we have investigated a new chemical link between alcohols and aldehydes through use of quantum chemistry paired with astrochemical models. Specifically, rather than focusing on a “bottom-up” formation route involving H-addition to grain-surface aldehydes, we here investigated a “top-down” route involving an initial reaction of an alcohol, in this case ethanol, with the halogens chlorine and in the gas phase. We find that, in particular, the formation of CH_3CHOH by this route is efficient, owing to barrierless reaction pathways, and subsequent gas-phase H-abstraction could efficiently yield acetaldehyde in cases where gas-phase ethanol is abundant. An examination of the calculated abundances of our models including these new reactions predicts peak abundances of CH_3CHOH comparable with that of the parent species ethanol, which was initially detected in Sgr B2 by Zuckerman et al. (1975). This finding suggests that CH_3CHOH may likewise represent a potential target for future studies in this or similar sources, though to our knowledge there is no spectroscopic data on this species.

There exist many potential future directions for this work. Firstly, further study of the subsequent reactions of the ethanol radicals is warranted. Moreover, experimental and theoretical studies of this and similar systems could verify whether or not this reaction route with halogens is accessible for a broad range of alcohols.

CONFLICT OF INTEREST STATEMENT

The authors declare that the research was conducted in the absence of any commercial or financial relationships that could be construed as a potential conflict of interest.

AUTHOR CONTRIBUTIONS

C.N.S. contributed to the the design, organization, writing of this work, and was both the main astrochemical modeler in addition to assisting with the quantum chemical calculations. G.M. helped as well with the design, conceptualization, and writing of this work, and performed the bulk of the quantum chemical calculations. D.W. and E.S. assisted with the astrochemical modeling. A.M.F. assisted in the review and writing of the manuscript, as well as with the astronomical background. A.R. similarly contributed to the overall project conceptualization and provided relevant astronomical data and background information.

FUNDING

The National Radio Astronomy Observatory and Green Bank Observatory are facilities of the U.S. National Science Foundation operated under cooperative agreement by Associated Universities, Inc. C.N.S., D.W., and E.S. gratefully acknowledge support through the Virginia Military Institute's Summer Undergraduate Research Institute (SURI) program. G.M acknowledges the support of the grant RYC2022-035442-I funded by MCIU/AEI/10.130 39/501100011033 and ESF+. G.M. also received support from project 20245AT016 (Proyectos Intramurales CSIC). We acknowledge the computational resources provided by the DRAGO computer cluster managed by SGAI-CSIC, and the Galician Supercomputing Center (CESGA). The supercomputer FinisTerrae III and its permanent data storage system have been funded by the Spanish Ministry of Science and Innovation, the Galician Government and the European Regional Development Fund (ERDF).

ACKNOWLEDGMENTS

C.N.S. thanks A. Byrne for compiling the model inputs used as a starting point for those used in this work.

DATA AVAILABILITY STATEMENT

The datasets generated by this work are available upon request to the corresponding author.

REFERENCES

Acharyya, K. and Herbst, E. (2017). Gas-grain Fluorine and Chlorine Chemistry in the Interstellar Medium. *The Astrophysical Journal* 850, 105. doi:10.3847/1538-4357/aa937e

Asgeirsson, V., Birgisson, B. O., Bjornsson, R., Becker, U., Neese, F., Riplinger, C., et al. (2021). Nudged Elastic Band Method for Molecular Reactions Using Energy-Weighted Springs Combined with Eigenvector Following. *Journal of Chemical Theory and Computation* 17, 4929–4945. doi:10.1021/acs.jctc.1c00462

Asplund, M., Grevesse, N., Sauval, A. J., and Scott, P. (2009). The Chemical Composition of the Sun. *Annual Review of Astronomy and Astrophysics* 47, 481–522. doi:10.1146/annurev.astro.46.060407.145222

Balucani, N., Ceccarelli, C., and Taquet, V. (2015). Formation of complex organic molecules in cold objects: the role of gas-phase reactions. *Monthly Notices of the Royal Astronomical Society* 449, L16–L20. doi:10.1093/mnrasl/slv009

Bartlett, R. J., Watts, J., Kucharski, S., and Noga, J. (1990). Non-iterative fifth-order triple and quadruple excitation energy corrections in correlated methods. *Chemical Physics Letters* 165, 513–522. doi:10.1016/0009-2614(90)87031-L

Belloche, A., Müller, H. S. P., Menten, K. M., Schilke, P., and Comito, C. (2013). Complex organic molecules in the interstellar medium: IRAM 30 m line survey of Sagittarius B2(N) and (M). *Astronomy and Astrophysics* 559, A47. doi:10.1051/0004-6361/201321096. Publisher: EDP ADS Bibcode: 2013A&A...559A..47B

[Dataset] Bjornsson, R. (2022). ASH – a multiscale modelling program. <https://ash.readthedocs.io/en/latest/>. Accessed: 2025-06-21

Bonfand, M., Belloche, A., Garrod, R. T., Menten, K. M., Willis, E., Stéphan, G., et al. (2019). The complex chemistry of hot cores in Sgr B2(N): Influence of cosmic-ray ionization and thermal history. *Astronomy & Astrophysics* 628, A27. doi:10.1051/0004-6361/201935523

Byrne, A. N., Xue, C., Voorhis, T. V., and McGuire, B. A. (2024). Sensitivity analysis of aromatic chemistry to gas-phase kinetics in a dark molecular cloud model. *Physical Chemistry Chemical Physics* 26, 26734–26747. doi:10.1039/D4CP03229B. Publisher: The Royal Society of Chemistry

Caldeweyher, E., Ehlert, S., Hansen, A., Neugebauer, H., Spicher, S., Bannwarth, C., et al. (2019). A generally applicable atomic-charge dependent London dispersion correction. *Journal of Chemical Physics* 150. doi:10.1063/1.5090222

Chesnavich, W. J. (1986). Multiple transition states in unimolecular reactions. *The Journal of Chemical Physics* 84, 2615–2619. doi:10.1063/1.450331. Publisher: American Institute of Physics

Das, A., Chakrabarti, S. K., Acharyya, K., and Chakrabarti, S. (2008). Time evolution of simple molecules during proto-star collapse. *New Astronomy* 13, 457–467. doi:10.1016/j.newast.2008.01.003. ADS Bibcode: 2008NewA...13..457D

Esteban, C., Peimbert, M., García-Rojas, J., Ruiz, M. T., Peimbert, A., and Rodríguez, M. (2004). A reappraisal of the chemical composition of the Orion nebula based on Very Large Telescope echelle spectrophotometry. *Monthly Notices of the Royal Astronomical Society* 355, 229–247. doi:10.1111/j.1365-2966.2004.08313.x

Garrod, R. T. (2013). A Three-phase Chemical Model of Hot Cores: The Formation of Glycine. *The Astrophysical Journal* 765, 60. doi:10.1088/0004-637X/765/1/60

Garrod, R. T., Wakelam, V., and Herbst, E. (2007). Non-thermal desorption from interstellar dust grains via exothermic surface reactions. *Astronomy and Astrophysics* 467, 1103–1115. doi:10.1051/0004-6361:20066704

Garrod, R. T., Weaver, S. L. W., and Herbst, E. (2008). Complex chemistry in star-forming regions: an expanded gas-grain warm-up chemical model. *The Astrophysical Journal* 682, 283

Georgievskii, Y., Miller, J. A., Burke, M. P., and Klippenstein, S. J. (2013). Reformulation and solution of the master equation for multiple-well chemical reactions. *Journal of Physical Chemistry A* 117, 12146–12154. doi:10.1021/jp4060704. Publisher: American Chemical Society

Gillan, M. J. (1987). Quantum-classical crossover of the transition rate in the damped double well. *Journal of Physics C: Solid State Physics* 20, 3621–3641. doi:10.1088/0022-3719/20/24/005. Publisher: IOP Publishing

Goto, M. (2013). The cosmic ray ionization rate in the central parsec of the Galaxy. *Proceedings of the International Astronomical Union* 9, 429–433. doi:10.1017/S1743921314001070

Grimme, S., Goerigk, L., and Fink, R. F. (2012). Spin-component-scaled electron correlation methods. *WIREs Computational Molecular Science* 2, 886–906. doi:10.1002/wcms.1110. Publisher: Wiley

Henkelman, G., Uberuaga, B. P., and Jónsson, H. (2000). Climbing image nudged elastic band method for finding saddle points and minimum energy paths. *Journal of Chemical Physics* 113, 9901–9904. doi:10.1063/1.1329672

Hill, J. G., Mazumder, S., and Peterson, K. A. (2010). Correlation consistent basis sets for molecular core-valence effects with explicitly correlated wave functions: The atoms B–Ne and Al–Ar. *The Journal of Chemical Physics* 132, 054108. doi:10.1063/1.3308483

Hiraoka, K., Yamashita, A., Miyagoshi, T., Oohashi, N., Kihara, Y., and Yamamoto, K. (1998). Reactions of Hydrogen Atoms with Solid, Thin Films of Acetone and 2-Propanol at 13 K. *The Astrophysical Journal* 508, 423–430. doi:10.1086/306385. Publisher: IOP ADS Bibcode: 1998ApJ...508..423H

Ioppolo, S., Fedoseev, G., Chuang, K.-J., Cuppen, H. M., Clements, A. R., Jin, M., et al. (2020). A non-energetic mechanism for glycine formation in the interstellar medium. *Nature Astronomy*, 1–9doi:10.1038/s41550-020-01249-0. Publisher: Nature Publishing Group

Jodkowski, J. T., Rayez, M.-T., Rayez, J.-C., Bérbes, T., and Dóbé, S. (1999). Theoretical Study of the Kinetics of the Hydrogen Abstraction from Methanol. 3. Reaction of Methanol with Hydrogen Atom, Methyl, and Hydroxyl Radicals. *The Journal of Physical Chemistry A* 103, 3750–3765. doi:10.1021/jp984367q

Kendall, R. A., Dunning, T. H., and Harrison, R. J. (1992). Electron affinities of the first-row atoms revisited. Systematic basis sets and wave functions. *The Journal of Chemical Physics* 96, 6796–6806. doi:10.1063/1.462569. Publisher: AIP Publishing

Kozuch, S. and Martin, J. M. (2011). DSD-PBEP86: In search of the best double-hybrid DFT with spin-component scaled MP2 and dispersion corrections. *Physical Chemistry Chemical Physics* 13, 20104–20107. doi:10.1039/c1cp22592h. Publisher: The Royal Society of Chemistry

Laas, J. C. and Caselli, P. (2019). Modeling sulfur depletion in interstellar clouds. *Astronomy and Astrophysics* 624, A108. doi:10.1051/0004-6361/201834446

Loomis, R. A., Zaleski, D. P., Steber, A. L., Neill, J. L., Muckle, M. T., Harris, B. J., et al. (2013). The Detection of Interstellar Ethanamine (CH₃CHNH) from Observations Taken during the GBT PRIMOS Survey. *The Astrophysical Journal* 765, L9. doi:10.1088/2041-8205/765/1/L9. Publisher: IOP ADS Bibcode: 2013ApJ...765L...9L

Marchione, D., Mancini, L., Liang, P., Vanuzzo, G., Pirani, F., Skouteris, D., et al. (2022). Unsaturated Dinitriles Formation Routes in Extraterrestrial Environments: A Combined Experimental and Theoretical Investigation of the Reaction between Cyano Radicals and Cyanoethene (C₂H₃CN). *Journal of Physical Chemistry A* 126, 3569–3582. doi:10.1021/acs.jpca.2c01802. Publisher: American Chemical Society

McClure, M. K., Rocha, W. R. M., Pontoppidan, K. M., Crouzet, N., Chu, L. E. U., Dartois, E., et al. (2023). An Ice Age JWST inventory of dense molecular cloud ices. *Nature Astronomy* 7, 431–443. doi:10.1038/s41550-022-01875-w. ADS Bibcode: 2023NatAs...7..431M

McGuire, B. A. (2018). 2018 Census of Interstellar, Circumstellar, Extragalactic, Protoplanetary Disk, and Exoplanetary Molecules. *The Astrophysical Journal Supplement Series* 239, 17. doi:10.3847/1538-4365/aae5d2

Molpeceres, G., Nguyen, T., Oba, Y., and Watanabe, N. (2025). Hydrogenation of acetaldehyde on interstellar ice analogs results in limited destruction. *Astronomy & Astrophysics* 694, A299. doi:10.1051/0004-6361/202451990. Publisher: EDP Sciences

Mondal, S. K., Gorai, P., Sil, M., Ghosh, R., Etim, E. E., Chakrabarti, S. K., et al. (2021). Is There Any Linkage between Interstellar Aldehyde and Alcohol? *The Astrophysical Journal* 922, 194. doi:10.3847/1538-4357/ac1f31. ADS Bibcode: 2021ApJ...922..194M

Nandi, A., Molpeceres, G., Gupta, P. K., Major, D. T., Kästner, J., Martin, J. M. L., et al. (2022). Quantum Tunneling in Computational Catalysis and Kinetics: Is it Really Important? In *Comprehensive Computational Chemistry* (Elsevier). submitted. doi:<https://doi.org/10.1016/B978-0-12-821978-2.00020-9>

Neese, F. (2000). Approximate second-order SCF convergence for spin unrestricted wavefunctions. *Chemical Physics Letters* 325, 93–98. doi:10.1016/S0009-2614(00)00662-X

Neese, F. (2022). Software update: The ORCA program system—Version 5.0. *WIREs Computational Molecular Science* 12. doi:10.1002/wcms.1606

Neese, F., Wennmohs, F., Becker, U., and Riplinger, C. (2020a). The ORCA quantum chemistry program package. *Journal of Chemical Physics* 152, 224108. doi:10.1063/5.0004608. Publisher: American Institute of Physics

Neese, F., Wennmohs, F., Becker, U., and Riplinger, C. (2020b). The ORCA quantum chemistry program package. *The Journal of Chemical Physics* 152, 224108. doi:10.1063/5.0004608

Neill, J. L., Bergin, E. A., Lis, D. C., Schilke, P., Crockett, N. R., Favre, C., et al. (2014). Herschel Observations of Extraordinary Sources: Analysis of the Full Herschel/HIFI Molecular Line Survey of Sagittarius B2(N). *The Astrophysical Journal* 789, 8. doi:10.1088/0004-637X/789/1/8. Publisher: IOP ADS Bibcode: 2014ApJ...789....8N

Neufeld, D. A., Wolfire, M. G., and Schilke, P. (2005). The Chemistry of Fluorine-bearing Molecules in Diffuse and Dense Interstellar Gas Clouds. *The Astrophysical Journal* 628, 260–274. doi:10.1086/430663

Neufeld, D. A., Zmuidzinas, J., Schilke, P., and Phillips, T. G. (1997). Discovery of Interstellar Hydrogen Fluoride 1. *The Astrophysical Journal Letters* 488, L141–L144. doi:10.1086/310942

Pechukas, P. and Light, J. C. (1965). On Detailed Balancing and Statistical Theories of Chemical Kinetics. *The Journal of Chemical Physics* 42, 3281–3291. doi:10.1063/1.1696411. Publisher: American Institute of Physics

Perrero, J., Ugliengo, P., Ceccarelli, C., and Rimola, A. (2023). Quantum mechanical modelling of the grain-surface formation of acetaldehyde on H₂O:CO dirty ice surfaces. *Monthly Notices of the Royal Astronomical Society* 525, 2654–2667. doi:10.1093/mnras/stad2459

Qasim, D., Fedoseev, G., Chuang, K.-J., He, J., Ioppolo, S., van Dishoeck, E. F., et al. (2020). An experimental study of the surface formation of methane in interstellar molecular clouds. *Nature Astronomy* 4, 781–785. doi:10.1038/s41550-020-1054-y

Qasim, D., Fedoseev, G., Chuang, K. J., Taquet, V., Lamberts, T., He, J., et al. (2019). Formation of interstellar propanal and 1-propanol ice: a pathway involving solid-state CO hydrogenation. *Astronomy and Astrophysics* 627, A1. doi:10.1051/0004-6361/201935217. Publisher: EDP ADS Bibcode: 2019A&A...627A...1Q

Raghavachari, K., Trucks, G. W., Pople, J. A., and Head-Gordon, M. (1989). A fifth-order perturbation comparison of electron correlation theories. *Chemical Physics Letters* 157, 479–483. doi:10.1016/S0009-2614(89)87395-6

Rimola, A., Taquet, V., Ugliengo, P., Balucani, N., and Ceccarelli, C. (2014). Combined quantum chemical and modeling study of CO hydrogenation on water ice. *Astronomy and Astrophysics* 572, A70. doi:10.1051/0004-6361/201424046. ADS Bibcode: 2014A&A...572A..70R

Ruaud, M., Wakelam, V., and Hersant, F. (2016). Gas and grain chemical composition in cold cores as predicted by the Nautilus three-phase model. *Monthly Notices of the Royal Astronomical Society* 459, 3756–3767. doi:10.1093/mnras/stw887

Santra, G., Sylwetsky, N., and Martin, J. M. L. (2019). Minimally Empirical Double-Hybrid Functionals Trained against the GMTKN55 Database: revDSD-PBEP86-D4, revDOD-PBE-D4, and DOD-SCAN-D4. *The Journal of Physical Chemistry A* 123, 5129–5143. doi:10.1021/acs.jpca.9b03157

Scibelli, S. and Shirley, Y. (2020). Prevalence of Complex Organic Molecules in Starless and Prestellar Cores within the Taurus Molecular Cloud. *The Astrophysical Journal* 891, 73. doi:10.3847/1538-4357/ab7375

Song, L. and Kästner, J. (2017). Tunneling Rate Constants for H₂CO+H on Amorphous Solid Water Surfaces. *The Astrophysical Journal* 850, 118. doi:10.3847/1538-4357/aa943e. Publisher: IOP ADS Bibcode: 2017ApJ...850..118S

Taketani, F., Takahashi, K., Matsumi, Y., and Wallington, T. J. (2005). Kinetics of the Reactions of Cl*(² P_{1/2}) and Cl(² P_{3/2}) Atoms with CH₃ OH, C₂ H₅ OH, *n*-C₃ H₇ OH, and *i*-C₃ H₇ OH at 295 K. *The Journal of Physical Chemistry A* 109, 3935–3940. doi:10.1021/jp050055t

Tsikritea, A., Diprose, J. A., Softley, T. P., and Heazlewood, B. R. (2022). Capture theory models: An overview of their development, experimental verification, and applications to ion–molecule reactions. *The Journal of Chemical Physics* 157, 060901. doi:10.1063/5.0098552

Vazart, F., Ceccarelli, C., Balucani, N., Bianchi, E., and Skouteris, D. (2020). Gas-phase formation of acetaldehyde: review and new theoretical computations. *Monthly Notices of the Royal Astronomical Society* 499, 5547–5561. doi:10.1093/mnras/staa3060

Watanabe, N. and Kouchi, A. (2002). Efficient Formation of Formaldehyde and Methanol by the Addition of Hydrogen Atoms to CO in H[TINF]2/[TINF]O-CO Ice at 10 K. *The Astrophysical Journal* 571, L173–L176. doi:10.1086/341412. Publisher: IOP Publishing

Williams, A. E., Hammer, N. I., and Tschumper, G. S. (2021). Relative energetics of CH₃CH₂O, CH₃CHOH, and CH₂CH₂OH radical products from ethanol dehydrogenation. *The Journal of Chemical Physics* 155, 114306. doi:10.1063/5.0062809

Woon, D. E. (2002). Modeling Gas-Grain Chemistry with Quantum Chemical Cluster Calculations. I. Heterogeneous Hydrogenation of CO and H₂CO on Icy Grain Mantles. *The Astrophysical Journal* 569, 541–548. doi:10.1086/339279. Publisher: IOP ADS Bibcode: 2002ApJ...569..541W

Yang, Y.-L., Green, J. D., Pontoppidan, K. M., Bergner, J. B., Cleeves, L. I., II, N. J. E., et al. (2022). CORINOS. I. JWST/MIRI Spectroscopy and Imaging of a Class 0 Protostar IRAS 15398–3359. *The Astrophysical Journal Letters* 941, L13. doi:10.3847/2041-8213/aca289. Publisher: The American Astronomical Society

Zaleski, D. P., Seifert, N. A., Steber, A. L., Muckle, M. T., Loomis, R. A., Corby, J. F., et al. (2013). Detection of E-Cyanomethanimine toward Sagittarius B2(N) in the Green Bank Telescope PRIMOS Survey. *The Astrophysical Journal* 765, L10. doi:10.1088/2041-8205/765/1/L10. Publisher: IOP ADS Bibcode: 2013ApJ...765L..10Z

Zheng, J. and Truhlar, D. G. (2012). Multi-path variational transition state theory for chemical reaction rates of complex polyatomic species: ethanol + OH reactions. *Faraday Discussions* 157, 59. doi:10.1039/c2fd20012k

Zmuidzinas, J., Blake, G. A., Carlstrom, J., Keene, J., and Miller, D. (1995). HC[CLC]I/[CLC] Absorption toward Sagittarius B2. *The Astrophysical Journal* 447. doi:10.1086/309570

Zuckerman, B., Turner, B. E., Johnson, D. R., Lovas, F. J., Fourikis, N., Palmer, P., et al. (1975). Detection of interstellar trans-ethyl alcohol. *The Astrophysical Journal Letters* 196, L99–L102. doi:10.1086/181753

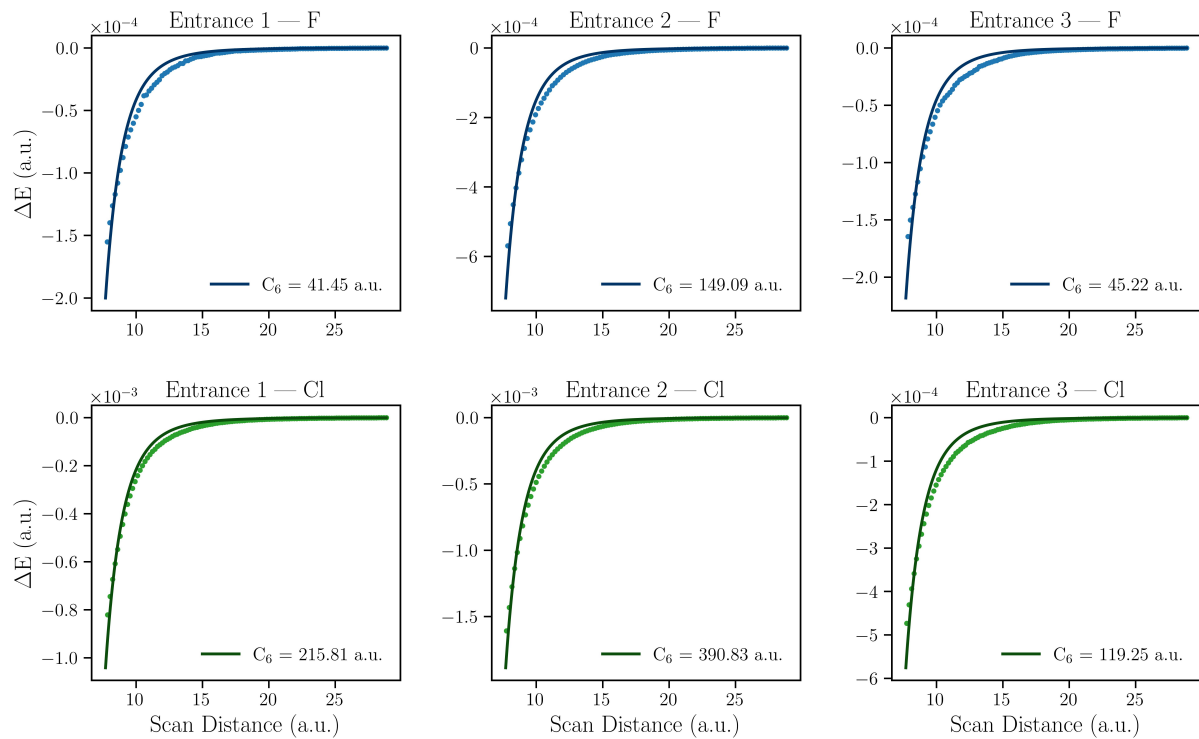


Figure 1. Capture rigid scans leading to PRCs or VDW complexes, see text. In the legend we show the value of the capture coefficient C_6 . The scans are not ZPE corrected.

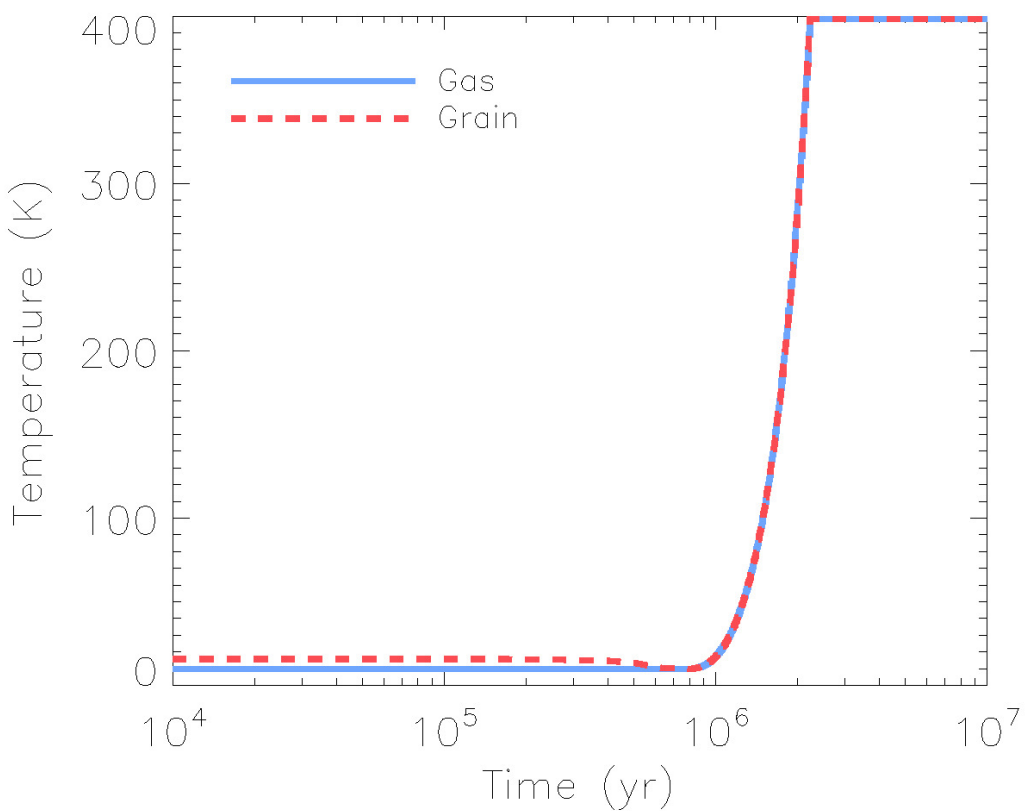


Figure 2. Gas and grain temperature evolution profiles.

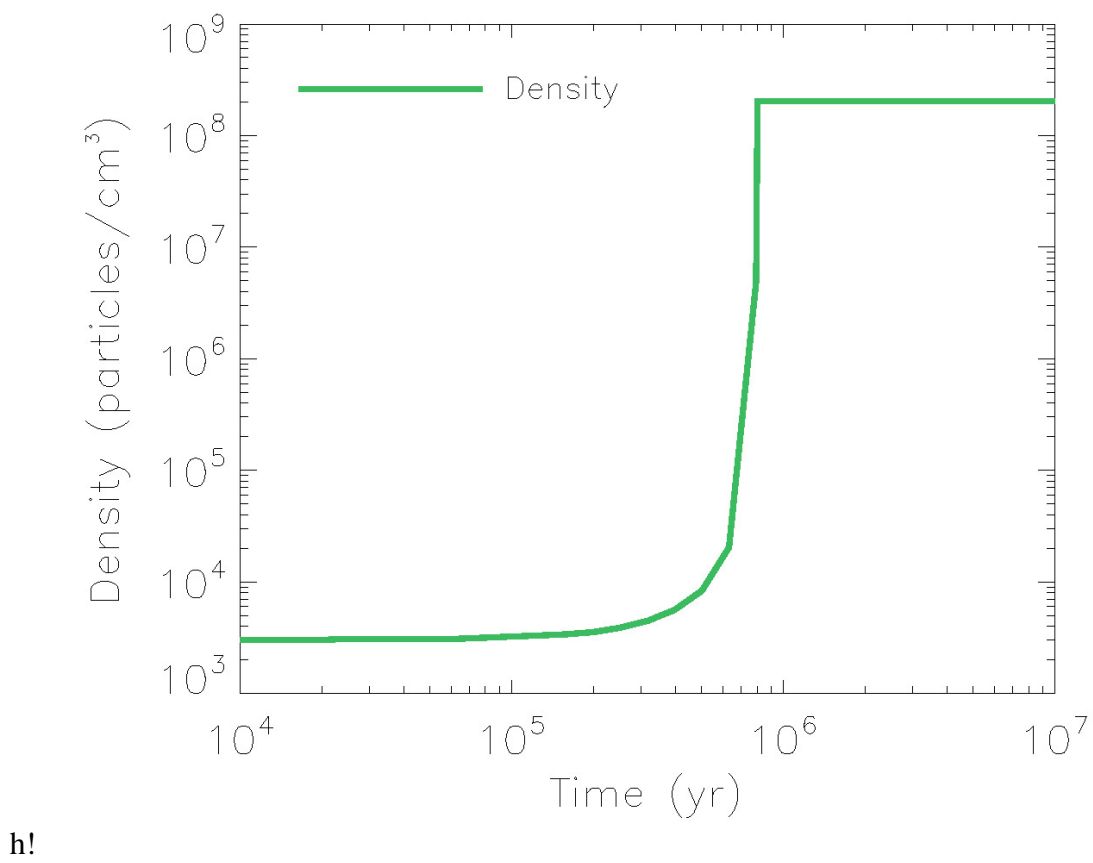


Figure 3. Density evolution profile.

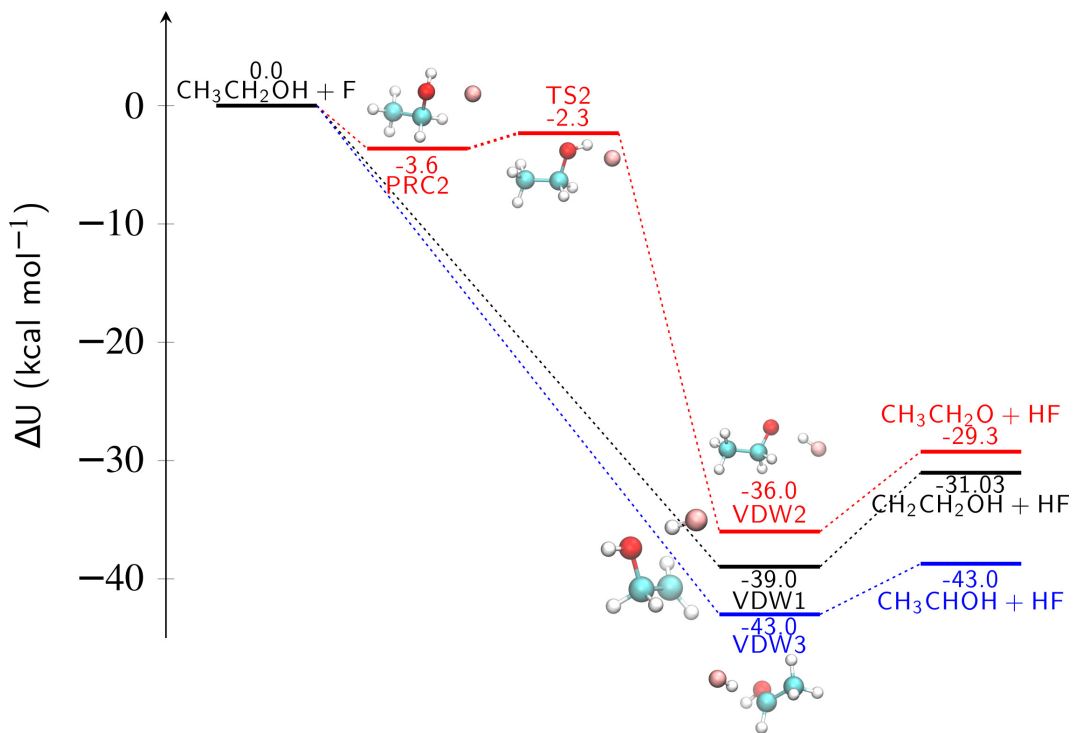


Figure 4. Potential energy profiles for the three abstraction channels in the $\text{CH}_3\text{CH}_2\text{OH} + \text{F}$ reaction. All energies are ZPVE corrected.

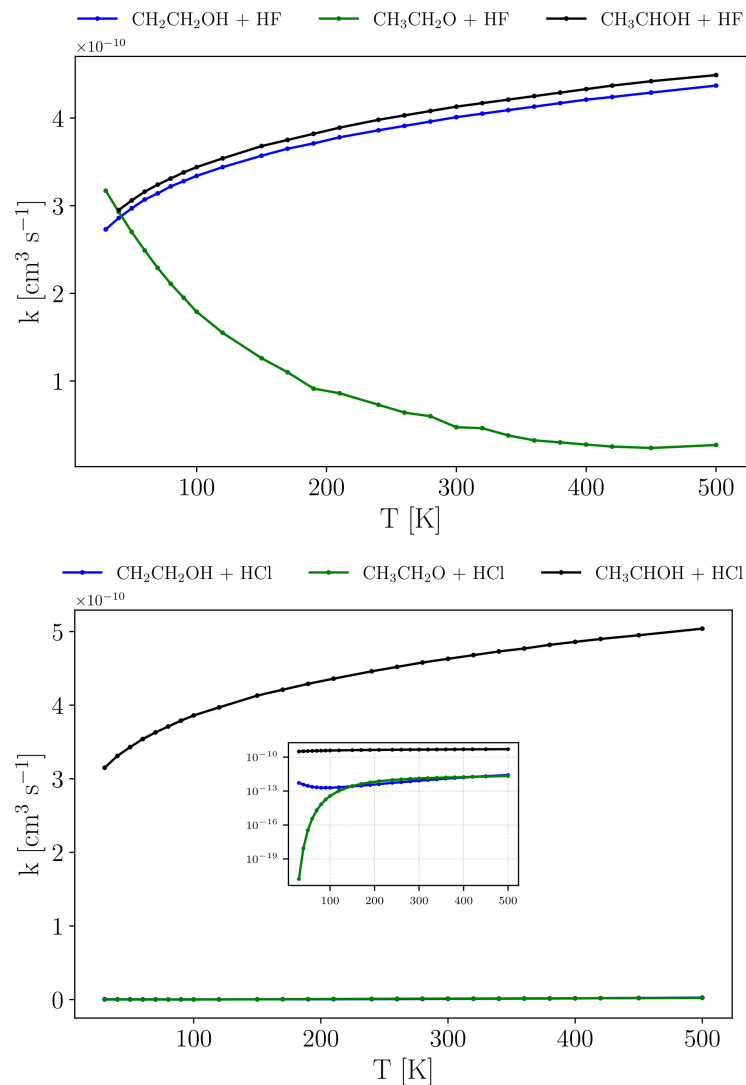


Figure 5. Reaction rate constants for the H-abstraction reactions of $\text{CH}_3\text{CH}_2\text{OH}$ with F (Top panel) and Chlorine (bottom panel)

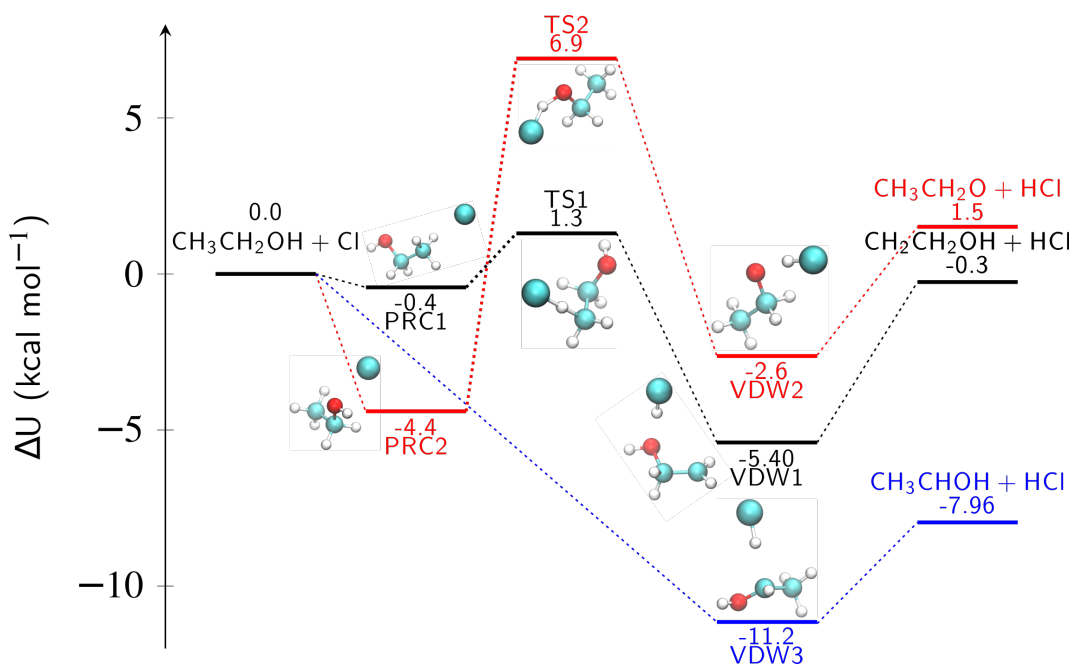


Figure 6. Potential energy profiles for the three abstraction channels in the $\text{CH}_3\text{CH}_2\text{OH} + \text{Cl}$ reaction. All energies are ZPVE corrected.

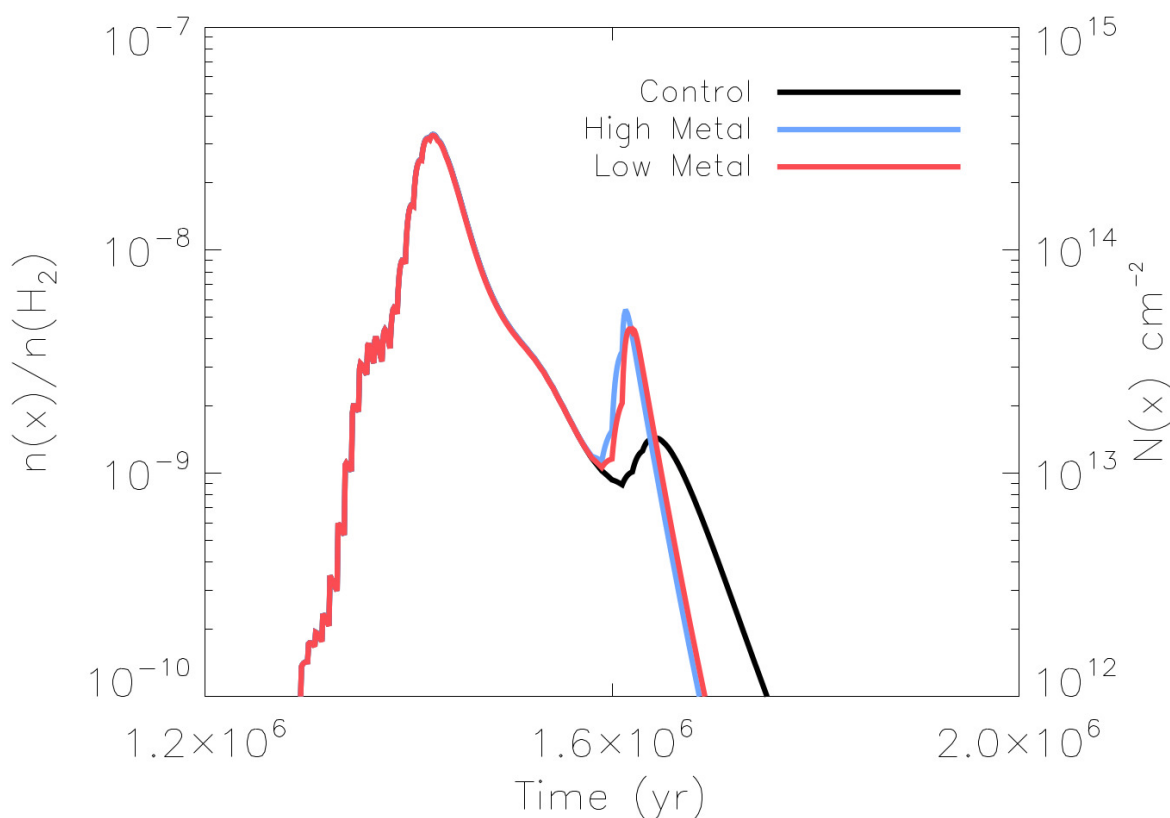


Figure 7. Abundances of CH_3CHO in our three-stage warmup model. Shown in black is the control model without the new reactions. Models including the new reactions are given in blue (high metal abundances) and red (low metal abundances).

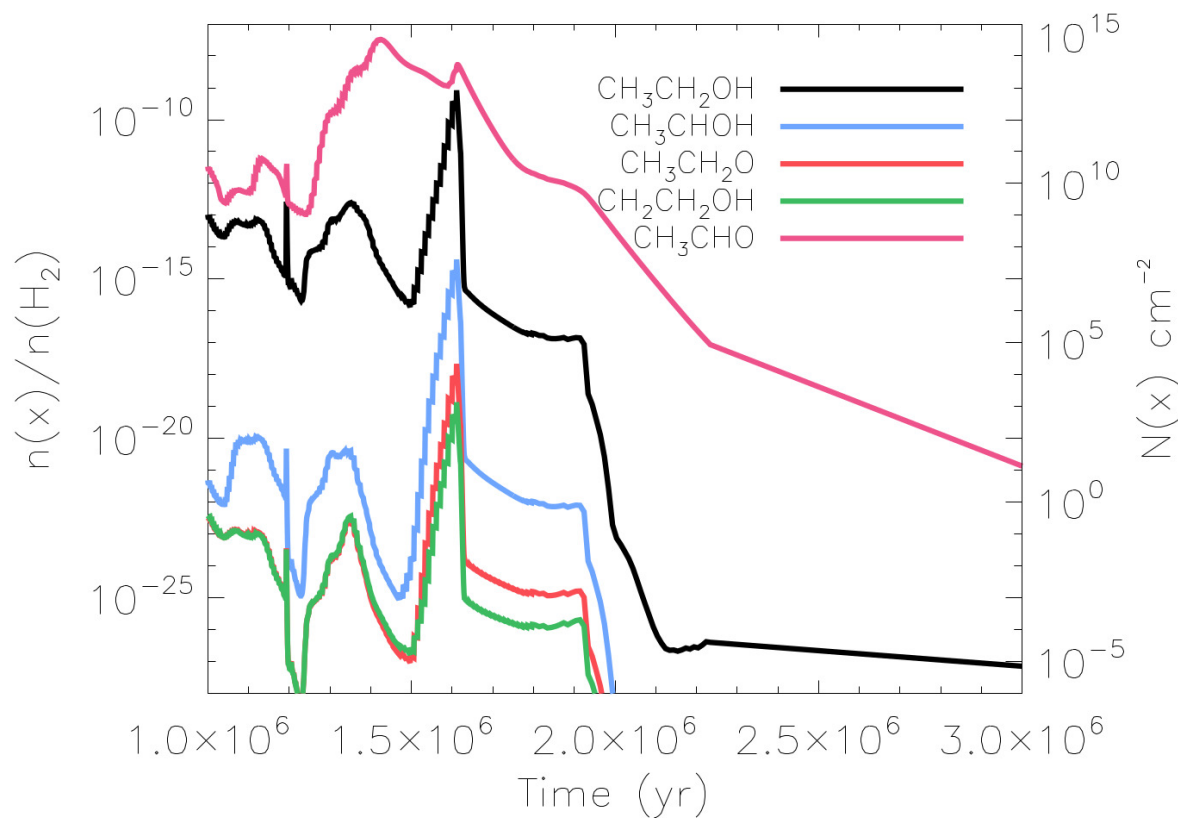


Figure 8. Abundances of $\text{CH}_3\text{CH}_2\text{OH}$, CH_3CHOH , $\text{CH}_3\text{CH}_2\text{O}$, $\text{CH}_2\text{CH}_2\text{OH}$, and CH_3CHO in our new model. Results shown here are for the high metal abundance model.